Observation of the Nuclear Magnetic Octupole Moment of ^{133}Cs

Vladislav Gerginov,[1] Andrei Derevianko,[2] and Carol E. Tanner[1]
[1]*University of Notre Dame, Department of Physics, Notre Dame, Indiana 46556, USA*
[2]*University of Nevada, Department of Physics, Reno, Nevada, 89557, USA*
(Received 4 March 2003; published 13 August 2003)

We describe our high-resolution measurements of the ^{133}Cs $6p\,^2P_{3/2}$ state hyperfine structure. An optically narrowed diode laser excites perpendicularly a highly collimated atomic beam. The spectra are calibrated with a stable reference diode laser using a rf locking scheme allowing us to determine the splittings with an accuracy of ≤ 2 kHz, an order of magnitude better than previous results. The magnetic dipole a, electric quadrupole b, and magnetic octupole c hyperfine coupling constants are determined. The values we obtained are $a = 50.288\,27(23)$ MHz, $b = -0.4934(17)$ MHz, and $c = 0.56(7)$ kHz. This work represents the first observation of the magnetic octupole moment of the cesium nucleus. We carry out atomic-structure calculations and determine the nuclear electric quadrupole moment $Q = -3.55(4)$ mb and nuclear magnetic octupole moment $\Omega = 0.82(10)$ b $\times\, \mu_N$.

DOI: 10.1103/PhysRevLett.91.072501 PACS numbers: 21.10.Ky, 27.60.+j, 32.10.Fn, 42.62.Fi

We report the precise measurements of the neutral ^{133}Cs $6p\,^2P_{3/2}$ state hyperfine splittings (HFS). The HFS result from electron-nuclear interactions and provide information about both the electronic and nuclear structure [1]. We anticipate that refined values of nuclear moments may provide better fitting parameters for models of nuclear forces, such as used in recent calculations for Cs [2,3].

Our HFS measurements must reach a precision of two parts in 10^{-5} in order to determine the nuclear magnetic octupole moment. Methods of optical-rf spectroscopy reach kHz accuracy [4] but states that decay through allowed transitions have lifetimes so short that high rf power, which could lead to systematic shifts, is required to redistribute the populations. For short-lived states, methods of polarization quantum beat spectroscopy [5] or laser frequency measurements in atomic beams [6] and thermal cells [7] have been successfully applied. The optical heterodyning technique we use here pushes the resolution of such measurements to ≤ 2 kHz, an order of magnitude better than previous results in Cs [6].

The $6p\,^2P_{3/2}$ state is sensitive to the magnetic dipole, electric quadrupole, and magnetic octupole interactions because the orbital quantum number $J = 3/2$. Our new values for the splittings are shown in Fig. 1. Using a laser system and atomic beam, we acquire well calibrated fluorescence spectra. From the data, the hyperfine interaction constants a, b, and c can be deduced. This is to our knowledge the first attempt to determine the nuclear magnetic octupole contribution, c, of the ^{133}Cs nucleus. We also carry out the atomic-structure calculations to determine the corresponding nuclear moments from our measurements. Previous determinations of magnetic octupole moments were carried out either with complicated open-shell atomic systems [8] or with multivalence electron systems [9]. In this regard, Cs, being a simple univalent atom, is a system where high-accuracy calculations can be performed.

A detailed description of our atomic beam appears elsewhere [10] and only a brief description is given here. Cs vapor is heated in an oven to 170 °C, while the Cs reservoir is kept at a lower temperature of 110 °C. The atoms effuse through a nozzle constructed from an array of stainless steel tubes to produce a dense atomic beam, which is then collimated with a stack of microscope cover slips. The resulting atomic beam has a 13×15 mm rectangular profile and angular divergence less than 13.6 mrad in the horizontal plane confirmed by the experimentally determined 2.3(1) MHz residual Doppler width of the spectral lines. The Cs atoms are excited with a 5 mm diameter $\sim 1\ \mu$W/cm^2 probe laser perpendicular to the atomic beam. The fluorescence intensity is detected with a large area photodiode placed below the laser-atom interaction region. A second detector monitors the transmission of the probe beam through the vacuum chamber to measure intensity, Cs background vapor, and atomic beam density (3×10^{13} cm^{-3}). The vacuum in the chamber with the beam running is 1.33×10^{-4} Pa.

Details of the laser system are described in Ref. [11] and a brief description is given here. An optically narrowed diode laser probes the $6s\,^2S_{1/2}\ F = 3, 4 \rightarrow 6p\,^2P_{3/2}\ F' = 2, 3, 4, 5$ transitions in the atomic beam. The probe beam is linearly polarized along the thermal beam. Part of the probe laser output is mixed with a

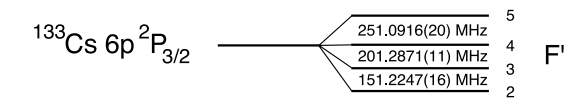

FIG. 1. Shown is the HF structure of ^{133}Cs $6p\,^2P_{3/2}$ state with our measured hyperfine splittings.

narrow linewidth reference diode laser beam and the beat note between the lasers is detected. The observed beat note is 100 kHz wide and limited by the resolution bandwidth of the spectrum analyzer, giving an upper limit on the linewidth of each laser of about 70 kHz. The reference laser is locked to a saturated absorption signal using a technique similar to that in [12]. The reference laser long term drift is estimated to be ≤ 30 kHz/h. The frequency difference between the lasers is locked to an rf oscillator. The probe laser can be scanned over a range of several hundred MHz by changing the rf oscillator frequency. The probe laser beam used for beat note measurements is frequency shifted by 80 MHz using an acousto-optic modulator (AOM). For $F = 3$ excitation, this beam is frequency shifted up by $\nu_{\mathrm{AOM}} = 80$ MHz, and the reference laser is locked to the $F = 3 \longrightarrow F' = 2$ transition. A frequency counter measures the difference ($\nu_{\mathrm{probe\ laser}} + \nu_{\mathrm{AOM}} - \nu_{\mathrm{ref\ laser}}$). For $F = 4$ excitation, the reference laser is locked to the $F = 4 \longrightarrow F' = 5$ transition and the beam used for beat note measurements is shifted down by $\nu_{\mathrm{AOM}} = 80$ MHz. The frequency counter measures the difference ($\nu_{\mathrm{ref\ laser}} - \nu_{\mathrm{probe\ laser}} + \nu_{\mathrm{AOM}}$). These shifts allow beat note measurements when the frequency of the probe beam is close to that of the reference laser.

The fluorescence and transmission detectors are connected to high-gain photodiode amplifiers. The amplifier output voltages are measured and averaged with a computer-based data acquisition system. The computer sets the rf oscillator to specific frequencies. A typical spectrum consists of 220 points when the excitation starts from the $F = 3$ and 230 points when ecitation starts from the $F = 4$ ground state. The fluorescence and transmission signals are read at a rate of 4000 samples/s until 2000 samples are collected. Simultaneously, the laser frequency difference is measured 100 times and averaged with the counter. Each data point contains the averaged value of the fluorescence and transmitted intensities with their standard deviations as well as the beat note frequency and its standard deviation. For a single point, the beat note standard deviation is between 15 and 25 kHz. Four spectra are recorded in one file, two of them with increasing and two with decreasing laser frequency. This is done in order to remove possible frequency drifts of the reference laser. The computer scans the probe laser with 0.5 MHz steps in the vicinity of a transition and with 10 MHz steps in between to reduce the scan acquisition time. This results in lower precision for the Lorentzian widths but does not affect the accuracy of the line center determined by the fit. A typical fluorescence spectrum with probe beam intensity of 1 μW/cm^2 is shown in Fig. 2.

The frequency dependence of our fluorescence spectra is well described by a Voigt profile and a thermally broadened Doppler profile to account for a Cs background [10]. In zero field with low excitation laser intensity, the contribution of Zeeman sublevels is a sum

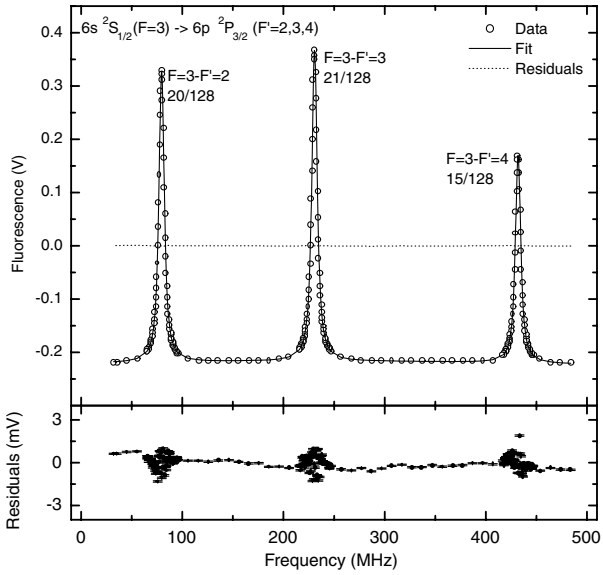

FIG. 2. Plot of the thermal beam fluorescence spectrum with excitation laser starting from $F = 3$ ground state. Circles: averaged fluorescence. Solid line: fit. Dashed line: residuals. Bottom trace: residuals magnified with uncertainties shown as error bars. Theoretical peak heights are also shown.

of Voigt profiles with relative peak heights determined by the angular momentum part of the transition probabilities. The low laser intensity and linear polarization minimize optical pumping that can create population differences between sublevels, and second-order effects such as off-resonant interactions with the lower $6p\,^2P_{1/2}$ state. The fitting process also includes an offset and a linear slope. A slope might be expected due to the 0.3% change of the laser intensity over the entire scan, but typically it is found to be close to zero since the amount of scattered laser light directly hitting the photodiode is negligibly small. The laser intensity change over the width of a transition is too small to be included in the line shape model. The amplified reverse voltage of the photodiode is responsible for the negative offset of all the spectra. It can differ over hours due to slow changes in detector temperature, but is found to be constant over a single scan (~ 2 min).

The Levenberg-Marquardt nonlinear fitting method is taken from [13]. The parameters obtained by fitting are the Voigt profile centers and amplitudes, the Lorentzian widths, the Doppler width, the Doppler background width, and the Doppler background proportionality parameter, the offset, and the linear slope. The averaged fluorescence signals and frequencies with their standard deviations are used by the fitting program (Fig. 2). Averaging the residuals over 100 data files for $F = 3$ excitation, we found the maximum asymmetric deviations from zero to be 0.25 mV (0.05%) for 0.5 V peak height several times less than a single file residuals. Similar spectra were taken with the excitation starting

from the $F = 4$ ground state. Averaging the residuals for 100 scans shows a maximum asymmetric deviation from zero of the order of 1 mV (0.1%) for a 1.1 V peak height. The small scatter in the residuals is due to reference laser instabilities which are transferred to the probe laser frequency and to mechanical vibrations of the thermal beam with respect to the probe beam with a period comparable to or greater than 0.5 s, the averaging time of the data acquisition system.

The peak centers for a single scan are determined with an accuracy of approximately 7 kHz. The Gaussian part of the profile is 2.3(1) MHz and the Lorentzian part is 5.5(1) MHz very close to the natural width of 5.23(1) MHz [14,15], but is slightly larger. Analysis shows that changing the density of points between the peaks changes the covariance between the Doppler and Lorentz widths of the peaks without changing the peak centers. This covariance alone can account for the slightly larger Lorentzian. Other possible contributions are the laser linewidth (70 kHz), power broadening (2.6 kHz), and time of flight broadening (2.4 kHz).

At laser intensities of 1 μW/cm^2 the typical atom is excited no more than once in its transit minimizing optical pumping, and the Stark shifts due to neighboring levels are ≤ 20 Hz. By making measurements over a range from 1 to 4 μW/cm^2 and from 1 to 70×10^{-6} Tesla dc magnetic field, we study possible systematic effects due to optical pumping and the Zeeman effect. With $B \leq 1 \times 10^{-6}$ T and $I = 4$ μW/cm^2, the largest change in the splittings is $\sim$6 kHz. With $B = 70 \times 10^{-6}$ T and $I = 4$ μW/cm^2, the largest change in the splittings is $\sim$10 kHz. With $B = 70 \times 10^{-6}$ T and $I = 1$ μW/cm^2, the largest change in the splittings is $\sim$4 kHz. With $B \leq 1 \times 10^{-6}$ T, the final value and statistical uncertainty for each splitting is obtained by averaging the values from 100 files for each laser intensity and extrapolating to zero intensity.

The small asymmetry in the residuals $\leq 0.1\%$ can be explained by tilt of the laser beam with respect to the atomic beam, leading to an upper limit on the systematic uncertainty in the splittings of approximately 1 kHz [10]. We combine this uncertainty in quadrature with the statistical uncertainty of the peak centers, which range from 1 to 2 kHz. The hyperfine splittings and their combined uncertainties are given in Table I. The consistency between the two measurements of the $3 \leftrightarrow 4$ splitting starting from different ground state levels is a good test of the reliability of our model and fitting process. Another test is the ratio between peak heights. Because of the long term variations in the thermal beam, it is not practical to compare peaks from different scans. But the ratios in the same file can be compared with theory. All peak height ratios agree with theory within 6%, and the small 3% difference between measured and theoretical ratios for the cycling transitions $(F = 3 \rightarrow F' = 2)/(F = 3 \rightarrow F' = 3)$ and $(F = 4 \rightarrow F' = 5)/(F = 4 \rightarrow F' = 4)$ gives confidence that we work at intensities low enough to limit optical pumping.

Using first-order perturbation theory, the hyperfine structure Hamiltonian of an atom having a single electron outside closed shells is given by [1]:

$$H_{\text{dipole}} = aI \cdot J, \qquad H_{\text{quadrupole}} = b\frac{3(I\cdot J)^2 + \frac{3}{2}(I\cdot J) - I(I+1)J(J+1)}{2I(2I-1)J(2J-1)},$$

$$H_{\text{octupole}} = c\frac{\{10(I\cdot J)^3 + 20(I\cdot J)^2 + 2(I\cdot J)[-3I(I+1)J(J+1) + I(I+1) + J(J+1) + 3] - 5I(I+1)J(J+1)\}}{I(I-1)(2I-1)J(J-1)(2J-1)},$$

where J is the electron angular momentum, I is the nuclear angular momentum, and F is the total angular momentum. Using the specific values of F, with $J = 3/2$ and $I = 7/2$, the hyperfine splittings of the $6p\,^2P_{3/2}$ state can be expressed in terms of the a, b, and c hyperfine constants:

$$\Delta\nu_{54} = 5a + \frac{5}{7}b + \frac{40}{7}c \; + \; (-0.000520 \text{ MHz}),$$

$$\Delta\nu_{43} = 4a - \frac{2}{7}b - \frac{88}{7}c \; + \; (+0.000119 \text{ MHz}),$$

$$\Delta\nu_{32} = 3a - \frac{5}{7}b + \frac{88}{7}c \; + \; (+0.000401 \text{ MHz}),$$

where the last term in each splitting is added because of the second-order perturbation theory contribution due to $6p\,^2P_{1/2}$ state [16]. Our measured values for a, b, and c are given in Table II.

Following the relativistic derivation given in [1], semiempirical estimations for the hyperfine coupling constants a, b, and c can be expressed through the magnetic dipole μ_I, electric quadrupole Q, and magnetic octupole Ω moments of the ^{133}Cs nucleus:

$$a_{lj} = \frac{\mu_0}{4\pi}\frac{2\mu_I\mu_B}{I}\frac{l(l+1)}{j(j+1)}\frac{(2j)(2j+1)(j+1)}{\rho(4\rho^2-1)}\left\langle\frac{1}{r^3}\right\rangle,$$

$$b_{lj} = \frac{e^2Q}{4\pi\varepsilon_0}\frac{2j-1}{2j+2}\frac{l(l+1)(2l+1)[3k(k+1) - \rho^2 + 1]}{\rho(\rho^2-1)(4\rho^2-1)}\left\langle\frac{1}{r^3}\right\rangle,$$

$$c_{1\frac{3}{2}} = \frac{\mu_0}{4\pi}\frac{16}{315}\mu_B\Omega\frac{Z^3Z_0^2}{a_B^5n^{*3}}\left(1 - \frac{d\sigma}{dn}\right)\frac{(2j+4)!\,(2\rho-4)!}{(2j-3)!\,(2\rho+3)!},$$

where μ_0 is the magnetic constant, $l = 1$, $j = 3/2$, $k = (-1)^{j+l-1/2}(2j+1)/2$, $\rho = \sqrt{k^2 - \alpha^2Z^2}$, α is the fine structure constant, Z is the nuclear charge reduced by

TABLE I. ^{133}Cs $6p\,^2P_{3/2}$ state hyperfine splittings in MHz from this work and previous measurement. The value of F shows the ground state component from which the measurement is performed.

	$2 \leftrightarrow 3$	$3 \leftrightarrow 4$	$4 \leftrightarrow 5$
$F = 3, 4$	151.2247(16)	201.2871(11)	251.0916(20)
$F = 3$	151.2247(16)	201.2876(12)	⋯
$F = 4$	⋯	201.2848(25)	251.0916(20)
Ref. [6]	151.21(2)	201.24(2)	251.00(2)

four for a p electron, $\langle 1/r^3 \rangle$ is the nonrelativistic radial matrix element:

$$\left\langle \frac{1}{r^3} \right\rangle = \left[(2l+1) \frac{\mu_0}{4\pi} \frac{\mu_B^2}{hc} \right]^{-1} \frac{Z Z_0^2 R_\infty \alpha^2}{l(l+1) n^{*3}} \left(1 - \frac{d\sigma}{dn} \right),$$

where $Z_0 = 1$ is the degree of ionization, n^* is the effective quantum number, σ is the quantum defect, n is the principal quantum number, and R_∞ is the Rydberg constant.

Using the data from [18], the parameters required to estimate the hyperfine coupling constants are $n^* = 2.363$, $d\sigma/dn = -0.059$, $\langle 1/r^3 \rangle = 1.36\, a_B^{-3}$. The value of $\mu_I = 2.582\,768\,1(14)\mu_N$ is taken from [19]. Our semiempirical estimations based on Ref. [1] are given in Table II.

The all-order relativistic many-body theory (MBPT) described in [17] results in a few percent accuracy for several well-known alkali atom constants a. Therefore we anticipate a similar accuracy for the constants b and c. Using this technique we calculate $b/Q = 139$ MHz/b and $c/\Omega = 0.68$ kHz/(b $\times\, \mu_N$). These MBPT values also appear in Table II. The theoretical uncertainty is estimated to be about 1%. Combining our MBPT results with our measured values of $b = -0.4934(17)$ MHz and $c = 0.56(7)$ kHz, we arrive at $Q = -3.55(4)$ mb and $\Omega = 0.82(10)$ b$\times\mu_N$ with experimental and theoretical uncertainties added in quadrature. The value of Q is in agreement with the value obtained through molecular measurements [20].

It is instructive to compare Ω with predictions of the nuclear shell model [21]. With an unpaired valence proton in the $g_{7/2}$ shell, $\Omega_{\text{n.s.m.}} = 0.095\langle r^2 \rangle_p \times \mu_N$, with the $\langle r^2 \rangle_p^{1/2}$ being the rms radius of the valence proton orbital. Roughly approximating this radius with the rms charge radius of $\langle r^2 \rangle^{1/2} = 4.807$ fm one arrives at $\Omega_{\text{n.s.m.}}(^{133}\text{Cs}) = 0.022$ b$\times\mu_N$. Compared to our inferred value, the nuclear shell model underestimates the magnetic octupole moment Ω by a factor of 40. The reason for this discrepancy is not clear and $\Omega(^{133}\text{Cs})$ may present an interesting test case for nuclear-structure calculations.

TABLE II. Hyperfine coupling constants a, b, and c from measured hyperfine splittings of ^{133}Cs $6p\,^2P_{3/2}$. First row: this work; second row: results obtained by Tanner *et al.* [6]. The third row represents the semiempirical estimations. The fourth row shows MBPT results.

a (MHz)	b (MHz)	c (kHz)
50.288 27(23)	−0.4934(17)	0.56(7)
50.275(3) [6]	−0.53(2) [6]	⋯
47.6	142 Q (b)	1.1 Ω (b $\times\, \mu_N$)
48.51 [17]	139 Q (b)	0.68 Ω (b $\times\, \mu_N$)

The authors would like to thank H. G. Berry, S. T. Ruggiero, A. E. Livingston, W. R. Johnson, L. Hollberg, and J. Bergquist for helpful discussions. Financial support for C. E. T. and V. G. was provided by the Division of Chemical Sciences, Office of Basic Energy Sciences, Office of Energy Research at the U.S. Department of Energy under Grant No. DE-FG02-95ER14579 and the National Science Foundation (NSF) under Grant No. PHY99-87984. The work of A. D. was supported in part by the NSF Grant No. 0099419 and a grant from the University of Nevada Junior Faculty Research Grant Fund. This support does not necessarily imply endorsement by any agency or university of the research conclusions.

[1] J. Lloyd Armstrong, in *Theory of the Hyperfine Structure of Free Atoms* (Wiley-Interscience, New York, 1971), 1st ed.
[2] D. Vretenar *et al.*, Phys. Rev. C **62**, 045502 (2000).
[3] P. K. Panda and B. P. Das, Phys. Rev. C **62**, 065501 (2000).
[4] W. J. Childs, Phys. Rep. **211**, 113 (1992).
[5] W. Yei, A. Sieradzan, and M. D. Havey, Phys. Rev. A **48**, 1909 (1993).
[6] C. E. Tanner and C. Wieman, Phys. Rev. A **38**, 1616 (1988).
[7] J. Ye, S. Swartz, P. Jungner, and J. L. Hall, Opt. Lett. **21**, 1280 (1996).
[8] W. J. Childs, Phys. Rev. A **44**, 1523 (1991).
[9] P. Kusch and T. G. Eck, Phys. Rev. **94**, 1799 (1954).
[10] V. Gerginov and C. E. Tanner, Opt. Commun. **222**, 17 (2003).
[11] V. Gerginov and C. E. Tanner, Opt. Commun. **216**, 391 (2003).
[12] R. W. Drever *et al.*, Appl. Phys. B **31**, 97 (1983).
[13] W. H. Press, S. A. Teukolsky, W. T. Vetterling, and B. P. Flannery, in *Numerical Recipes in Fortran 90* (Cambridge University Press, New York, 1996), 2nd ed.
[14] R. J. Rafac, C. E. Tanner, A. E. Livingston, and H. G. Berry, Phys. Rev. A **60**, 3648 (1999).
[15] A. Derevianko and S. G. Porsev, Phys. Rev. A **65**, 053403 (2002).
[16] W. Johnson (private communication).
[17] M. S. Safronova, W. R. Johnson, and A. Derevianko, Phys. Rev. A **60**, 4476 (1999).
[18] W. A. Van Wijngaarden and J. Li, J. Quant. Spectrosc. Radiat. Transfer **52**, 555 (1994).
[19] P. Raghavan, At. Data Nucl. Data Tables **42**, 189 (1989).
[20] M. Pernpointner, P. Schwerdtfeger, and B. A. Hess, J. Chem. Phys. **108**, 6739 (1998).
[21] C. Schwartz, Phys. Rev. **97**, 380 (1955).